Supplementary Information (SI) for Inorganic Chemistry Frontiers.
This journal is © the Partner Organisations 2025

Z-scheme heterojunction $ZnCdS/P_2W_{12}Fe_9AO$ nanocomposite based on an adsorption-photocatalytic strategy for efficient uranium reduction

*Yu Liu, Donghui Cui, Xue Yang, Fengyan Li**

Key Laboratory of Polyoxometalate and Reticular Material Chemistry of Ministry of Education, College of Chemistry, Northeast Normal University, Changchun 130024, P. R. China.

Email address: lify525@nenu.edu.cn

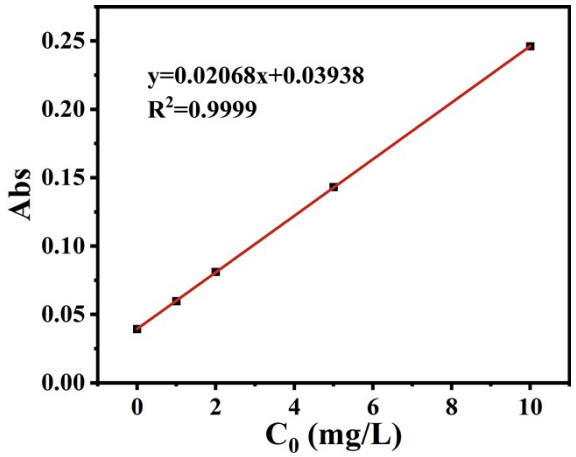

Fig. S1. Standard curve for the measurement of uranium by the Arsenazo III method.

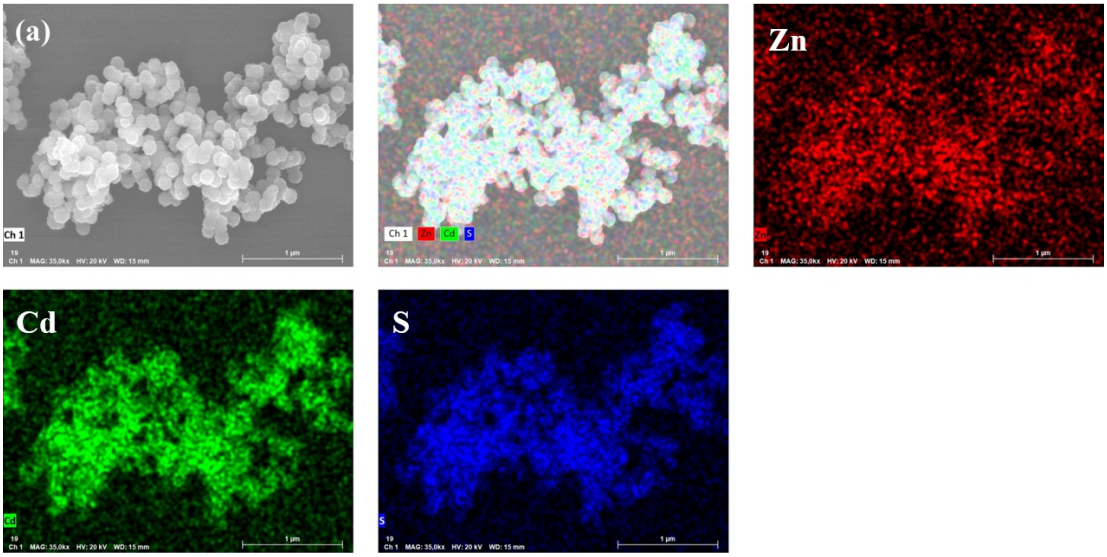

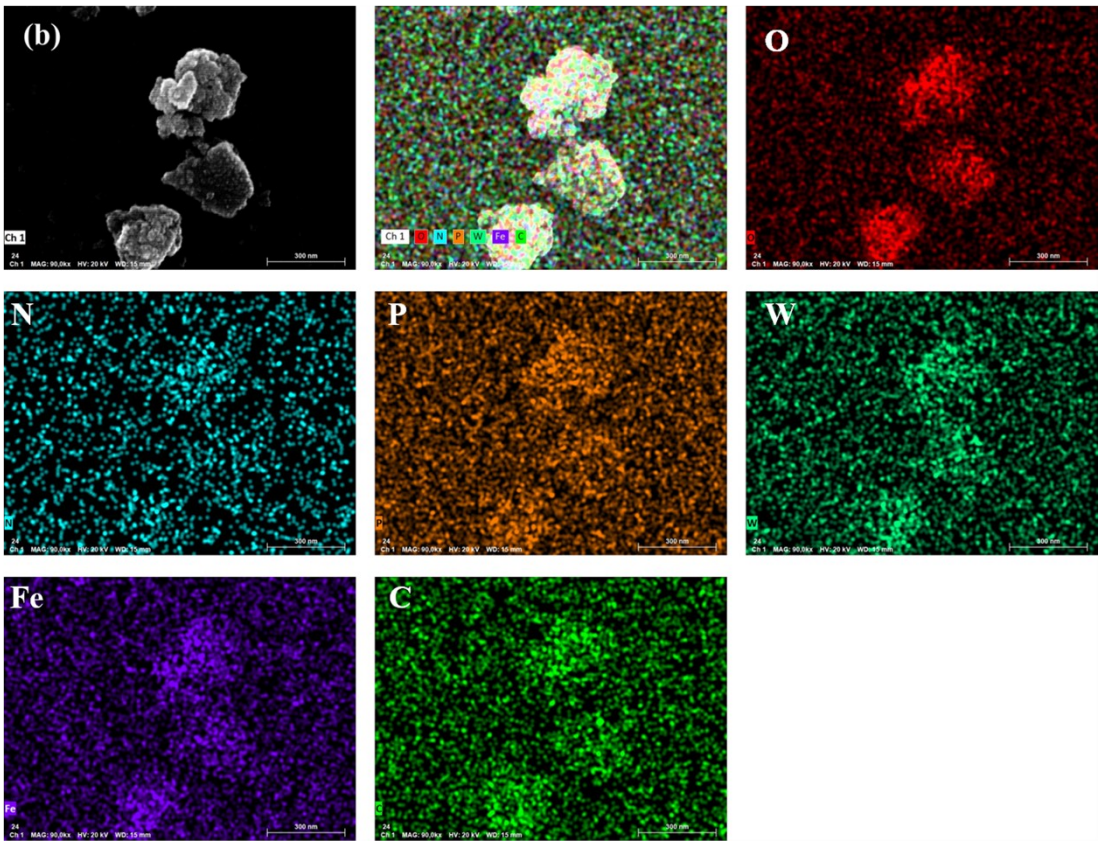
(b)
O
N
P
W
Fe
C

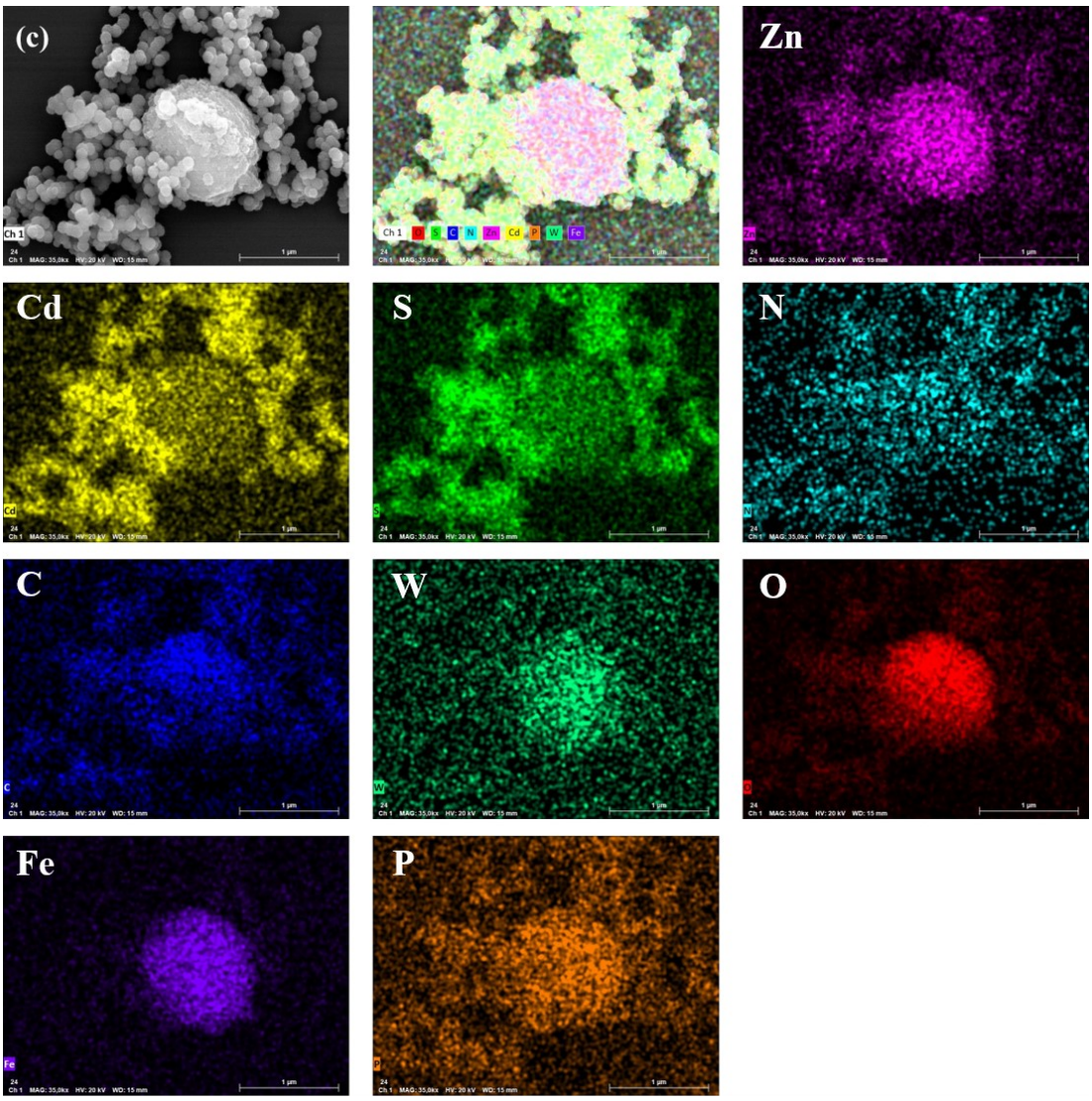
(c)
Zn
Cd
S
N
C
W
O
Fe
P

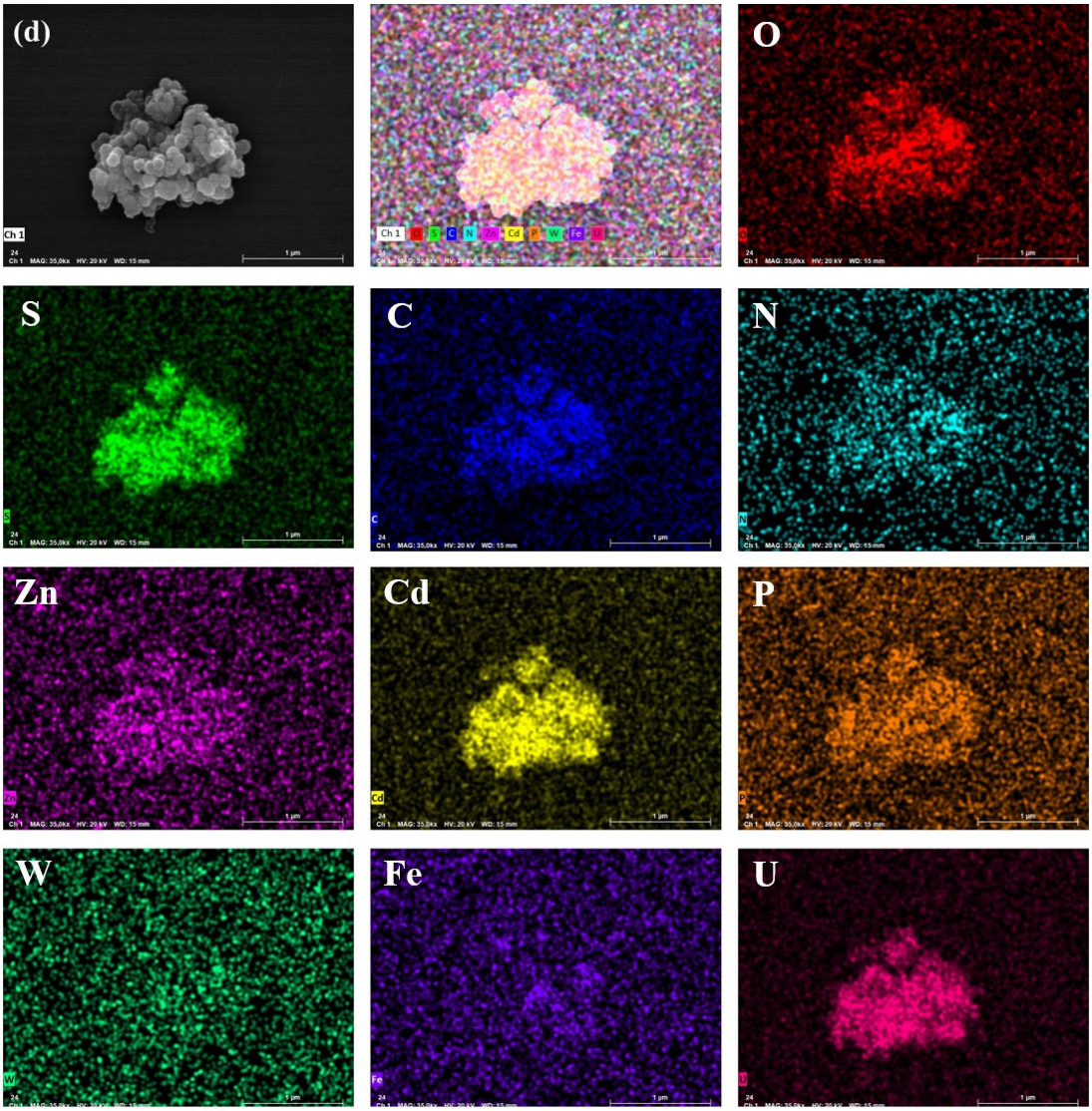

Fig. S2. (a) SEM elemental mapping images of ZnCdS. (b) $P_2W_{12}Fe_9AO$. (c) ZnCdS-$P_2W_{12}Fe_9AO$. (d) ZnCdS-$P_2W_{12}Fe_9AO$-U.

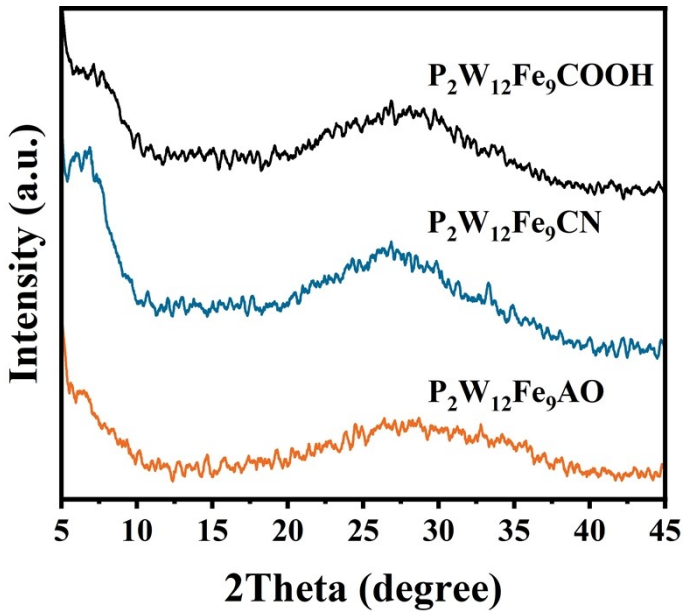

Fig. S3. XRD patterns of $P_2W_{12}Fe_9COOH$, $P_2W_{12}Fe_9CN$ and $PW_{12}AO$.

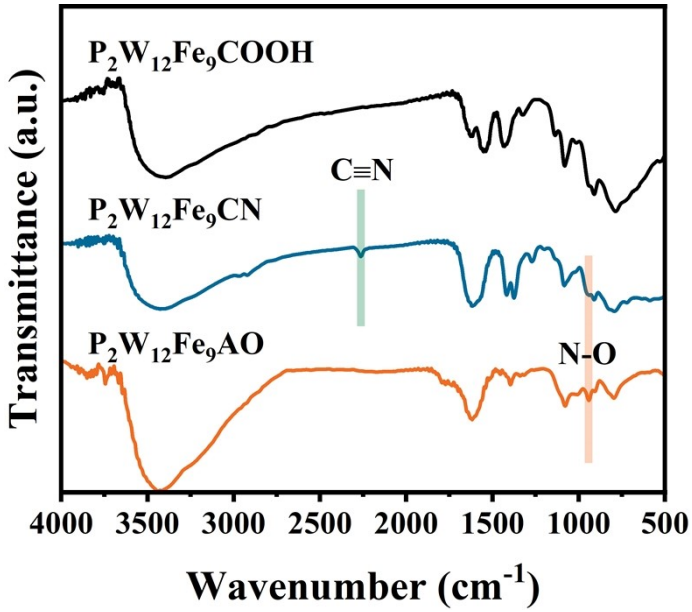

Fig. S4. FT-IR spectra of $P_2W_{12}Fe_9COOH$, $P_2W_{12}Fe_9CN$ and $PW_{12}AO$.

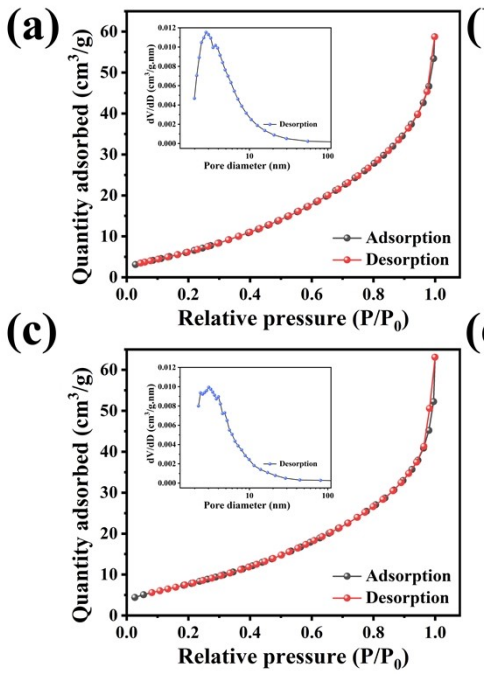

(d)

Samples	S_{BET} (m^2/g)	Pore volume (cm^3/g)	Pore size (nm)
ZnCdS	21.6	0.106	2.8
$P_2W_{12}Fe_9AO$	14.6	0.098	2.7
ZnCdS-$P_2W_{12}Fe_9AO$	26.6	0.107	3.0

Fig. S5. N_2 adsorption–desorption isotherms and Pore size distribution of ZnCdS, $P_2W_{12}Fe_9AO$, and ZnCdS-$P_2W_{12}Fe_9AO$.

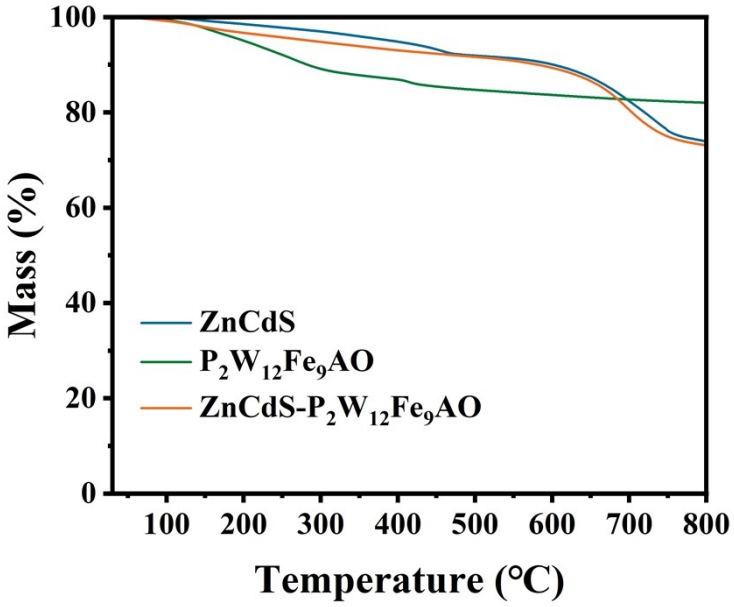

Fig. S6. TGA curves of ZnCdS, $P_2W_{12}Fe_9AO$, and ZnCdS-$P_2W_{12}Fe_9AO$ under N_2 atmosphere.

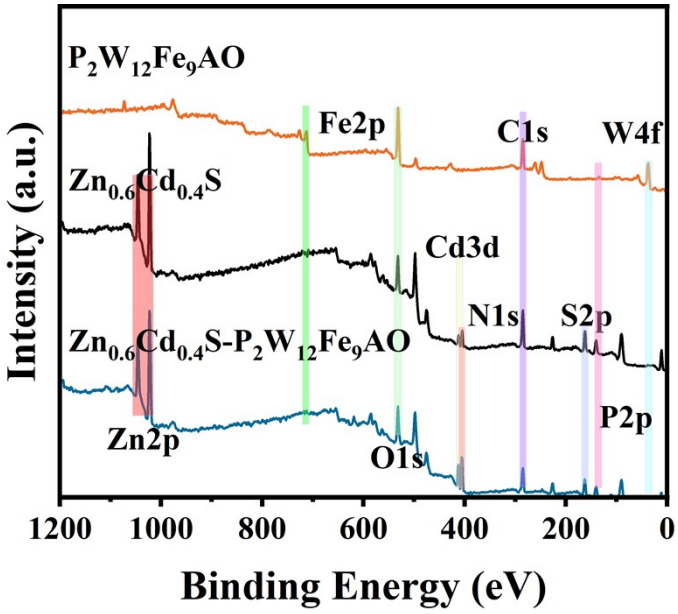

Fig. S7. XPS spectra of ZnCdS, $P_2W_{12}Fe_9AO$ and ZnCdS-$P_2W_{12}Fe_9AO$.

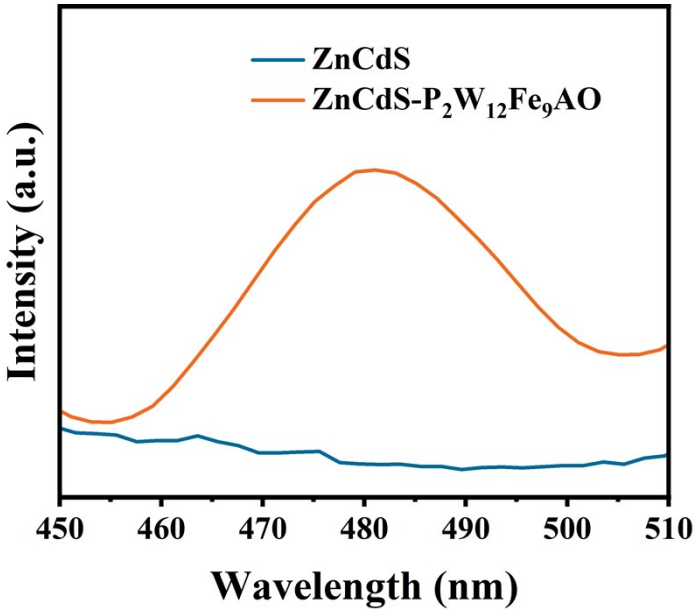

Fig. S8. Steady-state PL spectra of ZnCdS and ZnGd-$P_2W_{12}Fe_9AO$.

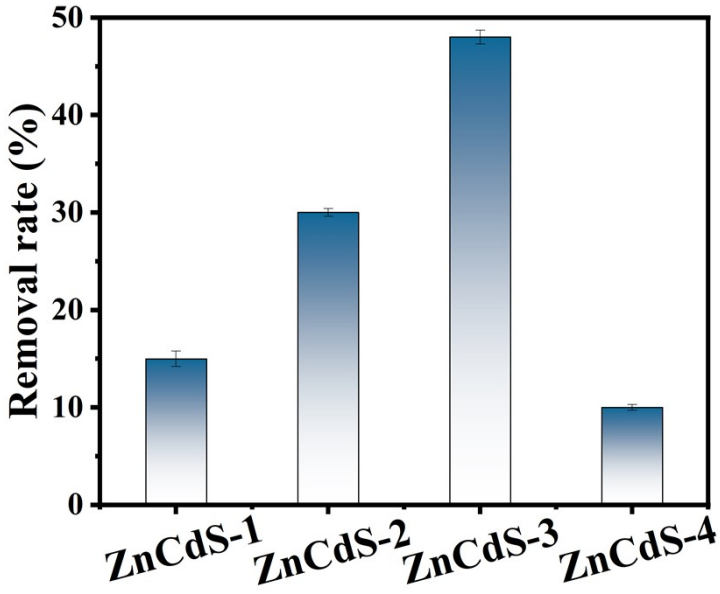

Fig. S9. Uranium removal performance of ZnCdS-1, ZnCdS-2, ZnCdS-3, and ZnCdS-4 (C_0 = 200 mg/L pH = 5).

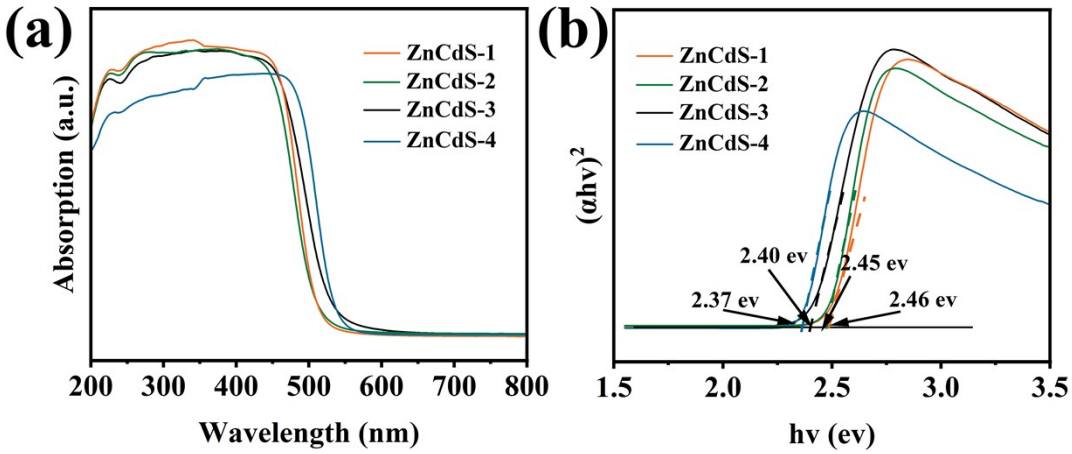

Fig. S10 (a) UV-vis DRS of ZnCdS-1, ZnCdS-2, ZnCdS-3, and ZnCdS-4. (b) Band gap of ZnCdS-1, ZnCdS-2, ZnCdS-3, and ZnCdS-4.

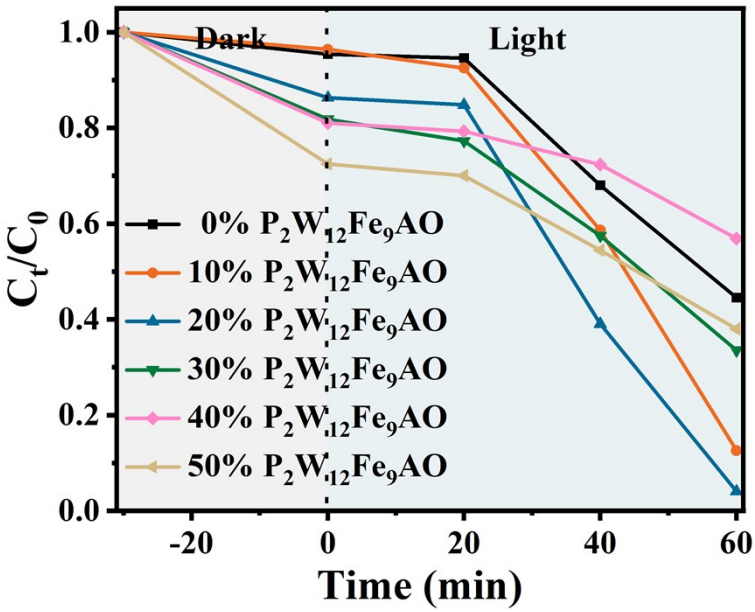

Fig. S11. Uranium removal performance of 0%$P_2W_{12}Fe_9AO$, 10%$P_2W_{12}Fe_9AO$, 20%$P_2W_{12}Fe_9AO$, 30%$P_2W_{12}Fe_9AO$, 40%$P_2W_{12}Fe_9AO$, and 50%$P_2W_{12}Fe_9AO$ (C_0 = 200 mg/L pH = 5).

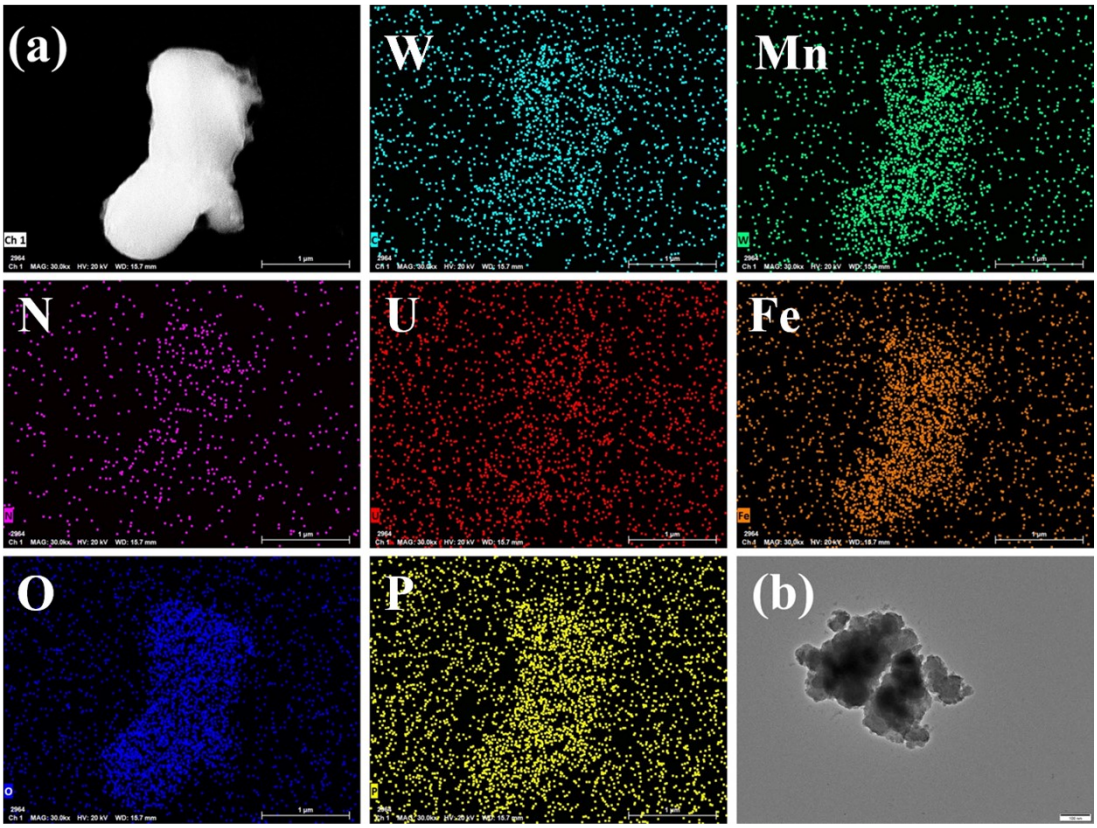

Fig. S12. (a) SEM elemental mapping images of $P_2W_{12}Fe_9AO$-U. (b) TEM of $P_2W_{12}Fe_9AO$-U.

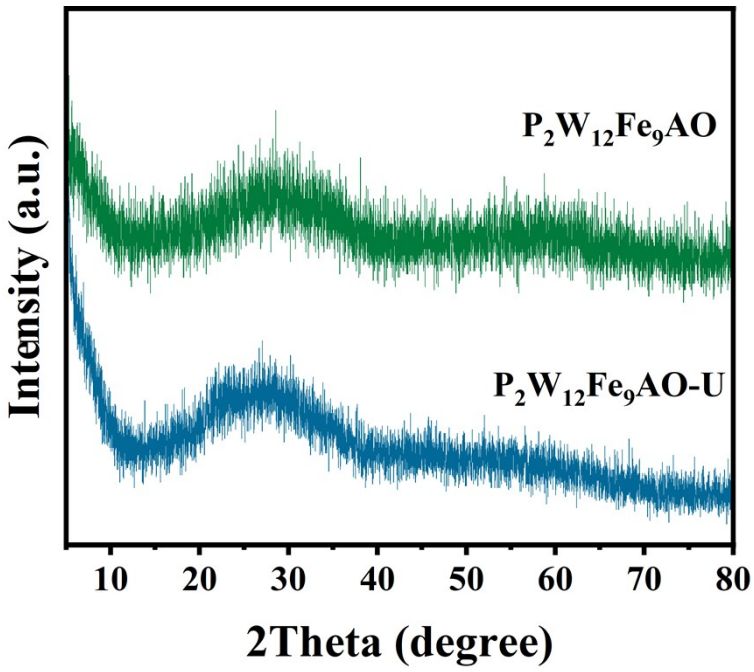

Fig. S13. (a) XRD patterns of $P_2W_{12}Fe_9AO$ and $P_2W_{12}Fe_9AO$-U.

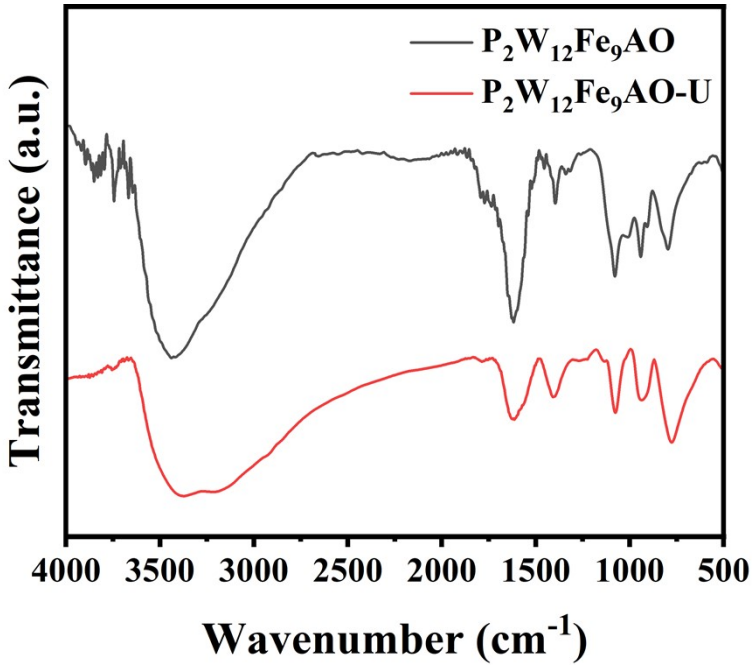

Fig. S14. FT-IR spectra of $P_2W_{12}Fe_9AO$ and $P_2W_{12}Fe_9AO$-U.

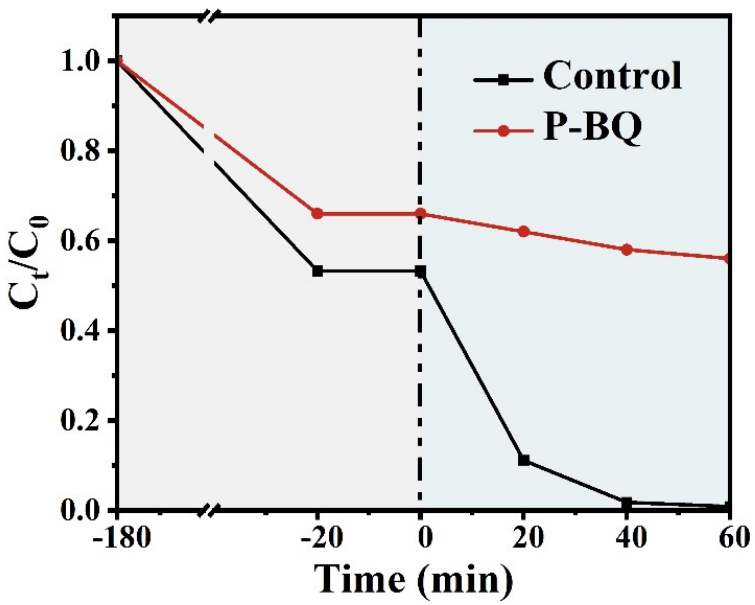

Fig. S15. The photocatalytic reduction of U(VI) over ZnCdS-$P_2W_{12}Fe_9AO$ with the additionof $\cdot O_2^-$ radical scavenger under visible light irradiation

Table S1 Comparison between the ZnCdS-$P_2W_{12}Fe_9AO$ and other photocatalysts.

Photocatalysts	$C_{U(VI)}$	RR (%)	Time	Hole trapping reagents	Ref.
$Gd(OH)_3/Cd_{0.8}Zn_{0.2}S$	50 mg/L	95.2%	180 min	No	1
$SrTiO_3/TiO_2$	100 mg/L	81.0%	180 min	No	2
$SnS_2/g\text{-}C_3N_4$	40 mg/L	92.7%	90 min	CH_3OH	3
$Br\text{-}C_3N_4$	200 mg/L	95%	60 min	CH_3OH	4
Fe-CN-3	50 mg/L	96.4%	240 min	CH_3OH	5
MoO_3 QDs/g-C_3N_4	50 mg/L	96.4%	150 min	CH_3OH	6
TT-TPP	200 mg/L	97.5%	600 min	No	7
ECUT-AQ	50 mg/L	86.0%	120 min	ascorbic acid	8

ZnCdS-$P_2W_{12}Fe_9AO$	250 mg/L	97.7%	120 min	No	This work

Table S2 Adsorption energy of $P_2W_{12}Fe_9CN$ and $P_2W_{12}Fe_9AO$ for U(VI).

Model	Adsorbate	Total energy (eV)	Slab energy (eV)	Molecular energy (eV)	Eads (eV)
$P_2W_{12}Fe_9CN$	UO_2^{2+}	-987.774	-956.396	-25.7627	-2.816
$P_2W_{12}Fe_9AO$	UO_2^{2+}	-1086.07	-1051.65	-25.7627	-7.011

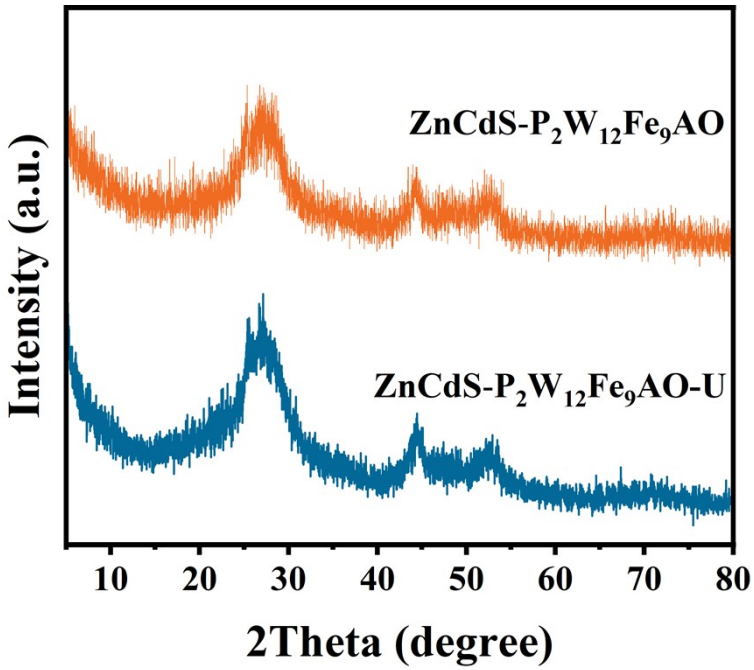

Fig. S16. XRD patterns of ZnCdS-$P_2W_{12}Fe_9AO$ and ZnCdS-$P_2W_{12}Fe_9AO$-U

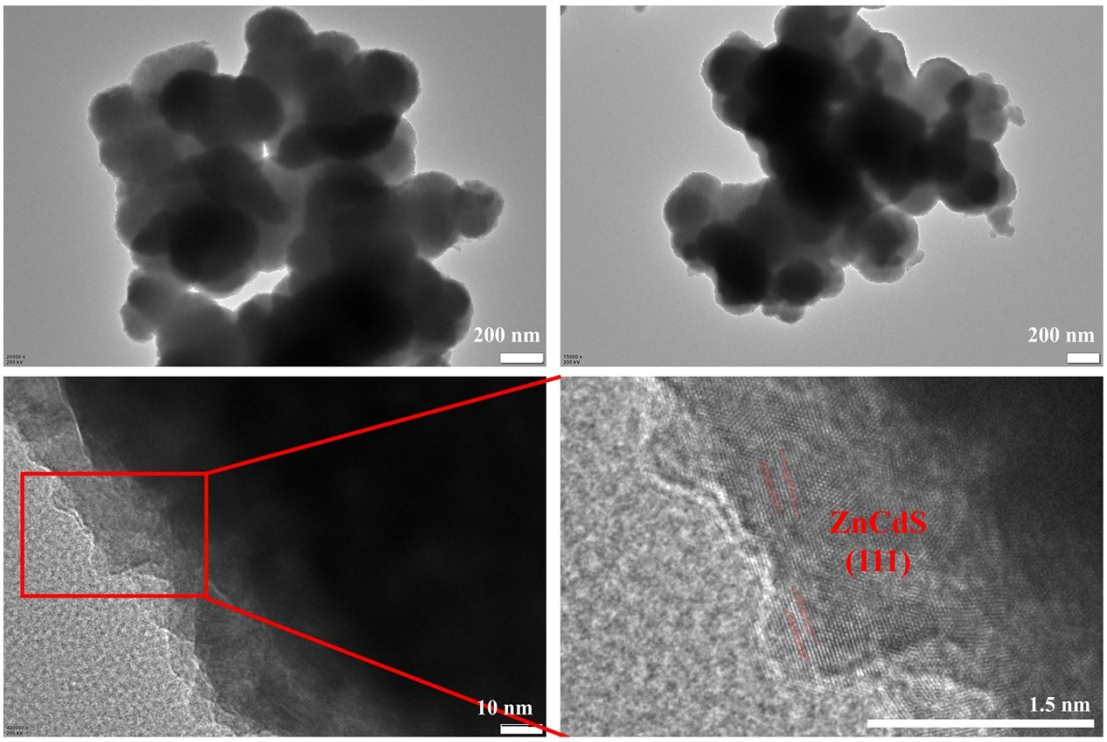

Fig. S17. TEM image of ZnCdS-$P_2W_{12}Fe_9AO$-U

References

1 W. Liu, Z. Yang, B. Zou, W. Liao, Y. Wang, C. Wang, S. Li, X. Niu, The photocatalytic application of $Gd(OH)_3/Cd_{0.8}Zn_{0.2}S$ nanocomposites in U (VI) reduction, Chem. Eng. J., 2023 **466** 143117.

2 L. Hu, X.-W. Yan, X.-J. Zhang, D. Shan, Integration of adsorption and reduction for uranium uptake based on $SrTiO_3/TiO_2$ electrospun nanofibers, Appl. Surf. Sci., 2018 **428** 819-824.

3 C. Liu, Z. Dong, C. Yu, J. Gong, Y. Wang, Z. Zhang, Y. Liu, Study on photocatalytic performance of hexagonal SnS_2/g-C_3N_4 nanosheets and its application to reduce U (VI) in sunlight, Appl. Surf. Sci., 2021 **537** 147754.

4 J. Xue, B. Wang, Z. Li, Z. Xie, Z. Le, Bromine doped g-C_3N_4 with enhanced photocatalytic reduction in U (VI), Res. Chem. Intermed., 2022 **48** 49-65.

5 W. Wei, Enhancing the photocatalytic performance of g-C_3N_4 by using iron single-atom doping for the reduction of U(VI) in aqueous solutions, J. Solid State Chem., 2022.

6 X. Zhu, Z. Dong, J. Xu, S. Lin, J. Liu, Z. Cheng, X. Cao, Y. Wang, Y. Liu, Z. Zhang, Visible-light induced electron-transfer in MoO_3 QDs/g-C_3N_4 nanosheets for efficient photocatalytic reduction of U(VI), J. Alloy. Compd., 2022 **926** 166609.

7 L. Chen, B. Chen, J. Kang, Z. Yan, Y. Jin, H. Yan, S. Chen, C. Xia, The synthesis of a novel conjugated microporous polymer and application on photocatalytic removal of uranium(VI) from wastewater under visible light, Chem. Eng. J., 2022 **431** 133222.

8 F. Yu, Z. Zhu, C. Li, W. Li, R. Liang, S. Yu, Z. Xu, F. Song, Q. Ren, Z. Zhang, A

redox-active perylene-anthraquinone donor-acceptor conjugated microporous polymer with an unusual electron delocalization channel for photocatalytic reduction of uranium (VI) in strongly acidic solution, Appl. Catal. B-Environ., 2022 **314** 121467.